

MODELING OF CERAMIC MICROSTRUCTURES: DYNAMIC DAMAGE INITIATION AND EVOLUTION

Horacio D. Espinosa and Pablo D. Zavattieri

*School of Aeronautics and Astronautics, Purdue University,
 West Lafayette, IN 47907*

A model is presented for the dynamic finite element analysis of ceramic microstructures subjected to multi-axial dynamic loading. This model solves an initial-boundary value problem using a multi-body contact scheme integrated with interface elements to simulate microcracking at grain boundaries and subsequent large sliding, opening and closing of interfaces. A systematic and parametric study of the effect of interface element parameters, grain anisotropy, stochastic distribution of interface properties, grain size and grain morphology is carried out. Numerical results are shown in terms of microcrack patterns and evolution of crack density. The qualitative and quantitative results presented in this article are useful in developing more refined continuum theories of fracture properties of ceramics.

INTRODUCTION

The influence of microscopic heterogeneities on the overall behavior of polycrystalline ceramics depends on morphological characteristics such as size, shape, lattice orientation and spatial distribution of different material properties. In our view, calculation of stress and strain distributions in real and idealized microstructures can increase the understanding of the different mechanisms that control macroscopic response. Furthermore, these micromechanical simulations can be useful for quantification and determination of failure mechanisms as well as the derivation of evolution equations to be used in continuum models (1).

COMPUTATIONAL MODEL

A micro-mechanical finite element modeling of ceramic microstructures under dynamic loading is presented to assess intergranular microcrack

initiation and evolution. A representative volume element of an actual microstructure, subjected to compression-shear dynamic loading, is considered for the analysis. A large deformation elastic-anisotropic visco-plasticity model for the grains, incorporating grain anisotropy by randomly generating principal material directions, is included. Cohesive interface elements are embedded along grain boundaries to simulate microcrack initiation and evolution. Their interaction and coalescence is a natural outcome of the calculated material response.

Figure 1 shows a schematic of the multi-body contact-interface algorithm. A real ceramic microstructure is digitized to represent the grain morphology. Each grain is individually represented by a mesh with six noded triangular finite elements generated using Delaunay triangulations, and four-noded interface elements inserted at the grain boundary. See (2) for more details.

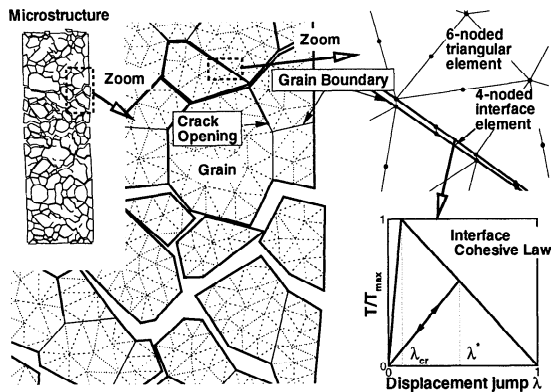


FIGURE 1: Schematics of microcracking at grain boundaries using the irreversible interface cohesive law showing the evolution of the traction with loading and unloading.

**CASE STUDY:
PRESSURE-SHEAR EXPERIMENT**

Plate impact experiments offer unique capabilities for the characterization of advanced materials under dynamic loading conditions, see (3). These experiments allow high stresses, high pressures, high strain rates and finite deformations to be generated under well characterized conditions. Compression-shear loading is attained by inclining the flyer, specimen, and target plates with respect to the axis of the projectile (see Fig. 2).

The specimen is a thin wafer of $540 \mu m$, sandwiched between two anvil plates, (i.e. the flyer and the target). In this configuration the flyer hits the specimen, which is attached to the target, with an initial velocity $V_0 = 148 m/s$. The angle of inclination in this case is $\gamma = 18^\circ$.

For a microstructural analysis of the pressure-shear configuration, a representative volume element is selected. The flyer-specimen interface is located at $y = H$, while the specimen-target interface is at $y = 0$. Periodic boundary conditions are applied. Furthermore, assuming that the target and flyer plates remain elastic through out the deformation process, the computational effort can be minimized by replacing the flyer and anvil plates with viscous boundary condi-

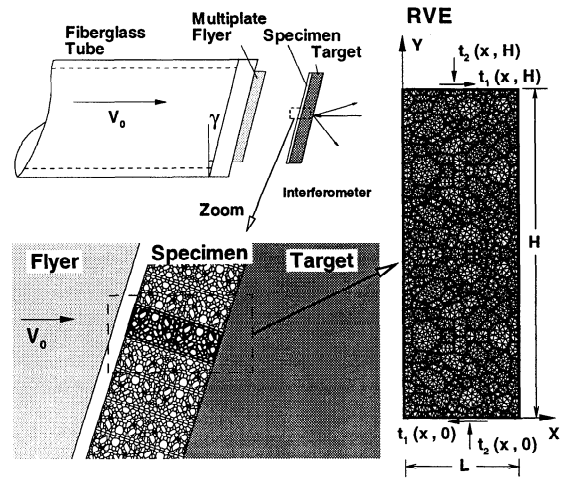


FIGURE 2: Schematics of the experimental configuration and the representative volume element.

tions based on one dimensional elastic wave theory.

RESULTS AND DISCUSSION

We shall focus on the study of the variation of geometrical and physical parameters that characterize the ceramic microstructure and their effect on the material response.

Effect of maximum interface strength T_{max} and material toughness K_{IC}

Six cases were studied, for two different values of K_{IC} (1.7 and $4 MPa \cdot m^{1/2}$) and three different values of T_{max} ($1, 5$ and $10 GPa$)

Figure 3 shows the crack pattern for each one of these six cases at 100 nanoseconds. In these sequences we can appreciate the different extent of crack nucleation and crack propagation. For the case with $K_{IC} = 1.7 MPa \cdot m^{1/2}$ and $T_{max} = 1 GPa$, most interface elements are broken as the wave advances. On the contrary, with the same K_{IC} and $T_{max} = 10 GPa$ a dilute distribution of cracks is achieved. It should be pointed out that $10 GPa$ represents a cohesive strength close to the theoretical $E/20$, in other words, grain boundaries without impurities and good lattice

matching.

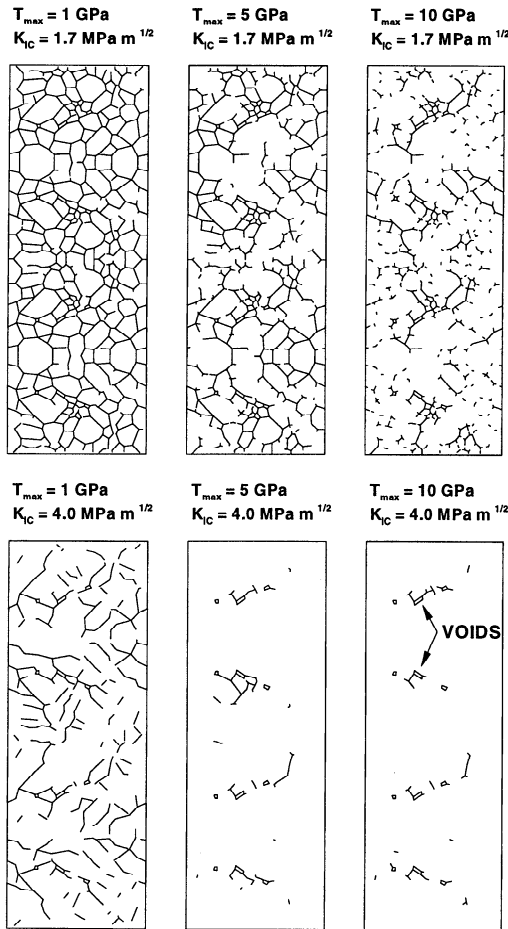


FIGURE 3: Crack pattern for different values of material toughness and interfacial strength.

The case with $K_{IC} = 4\text{MPa} \cdot \text{m}^{1/2}$ and $T_{max} = 1\text{GPa}$ presents a different crack pattern from all the other cases. The cases with $K_{IC} = 4\text{MPa} \cdot \text{m}^{1/2}$ and higher values of the interface strength, T_{max} , experience interface element breakage only at the corner of pre-existing voids, showing the effect of stress concentration and void collapse.

Although crack patterns give the possibility of understanding the process of microfracture inside the ceramic, the use of stereology provides more insight of the different damage mechanisms. For the case of nu-

merical simulations, the microcrack surface area per unit volume is directly defined as $S_v(t) = \text{total crack length}/\text{Area}$. Figure 4 shows the crack length per unit area, $S_v(t)$, as a function of time for each one of these six cases. The evolution of the crack density is more evident for the cases with weak interfaces.

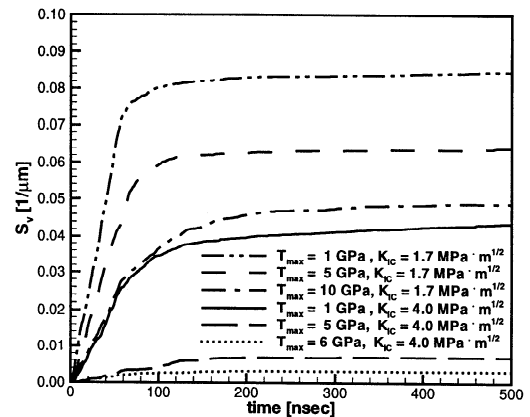


FIGURE 4: $S_v(t)$ for different values of material toughness and interfacial strength.

Unloading is simulated by removing the traction boundary conditions on the top and bottom surface of the specimen. Figure 5 shows the pulverization pattern for each one of these cases at 400 nanoseconds after unloading. As discussed in (3), ceramics are so susceptible to fragmentation, that they represent the most difficult problems in wave propagation investigation with specimen recovery. These calculations have demonstrated that the pressure-shear configuration presented in Espinosa et al. (3) will be more attractive for recovery experiments of other materials, with higher toughness, in which damage, plasticity, or phase transformation induced by lateral wave release is minimized. If one accounts for the periodicity of the RVE, a clear picture of ceramic pulverization is inferred from these calculations.

Effect of grain elastic anisotropy

In this section we will study the stochastic effect of grain elastic anisotropy and its impact

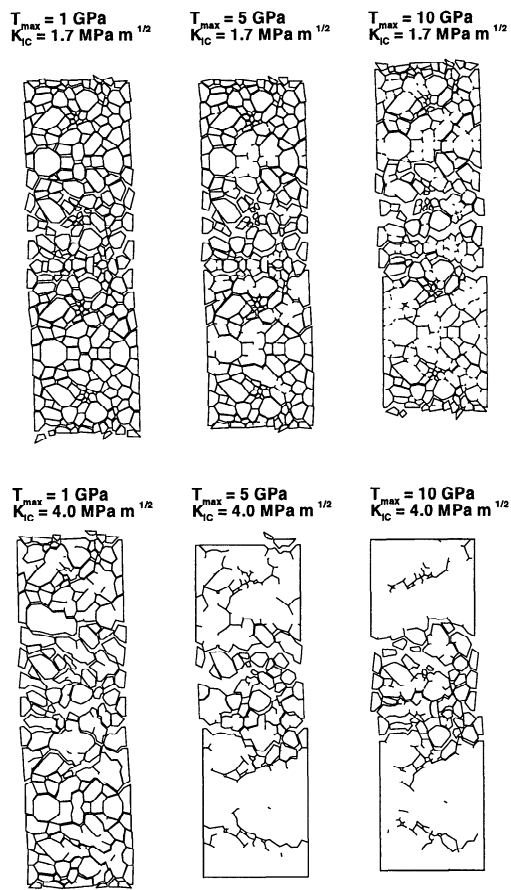


FIGURE 5: Pulverization pattern for different values of K_{IC} and T_{max} .

on the fracture behavior of the ceramic at the microlevel. Four identical microstructures are considered for this analysis. The only difference between each other is the fact that the principal material directions are generated randomly in three of them while only isotropic elasticity, average values for the polycrystalline material, is considered for the fourth case. This parametric study allows to see if the fact that each grain has random principal material directions presents significant variations in the RVE response. Also it addresses the question of what is the effect of this misorientation on intergranular crack regardless of the interfacial strength.

A clear tendency for higher values of S_v for the anisotropic cases has been obtained, see (2) for details. The standard deviation of the maximum value of S_v for the anisotropic cases has been found to be small compared with the variation of 20% between the anisotropic cases and the isotropic case.

Figure 6 can provide even more information on the microcrack evolution. At triple points, stress concentration is more important where the grains are described by different principal material directions. For the isotropic case, stress concentration is minimum. Future studies will focus on the effect of residual stresses, introduced during cooling from the sintering temperature, in the mechanical response of ceramics.

Effect of grain size

In addition, an analysis comparing a microstructure with smaller grain size has been carried out. In all the previous simulations the average grain size of the microstructure was $22 \mu m$. A second microstructure, with an average grain size of $11 \mu m$, was simulated under the same conditions in order to study the evolution of the crack density. It was observed that the maximum S_v is 35 % smaller in the case with smaller grains.

Effect of stochastic distribution of interface properties

The random distribution of glass pockets, glassy phases, *SiC* nanoparticles, defects and other impurities leads to the consideration of a statistical variation in the interfacial strength dependent on the grain misorientation. Data on grain boundary toughness as a function of coincident lattice sites are very limited and incomplete in the literature. For this reason we have done an analysis of the stochasticity of the microfracture process with distributions which are independent of the principal material directions.

In this analysis, the interfacial strength parameters will be described by a *Weibull* or *Gaussian* distribution. Since we can only vary two interface parameters, we will consider two distributions: varying K_{IC} and keeping T_{max} constant,

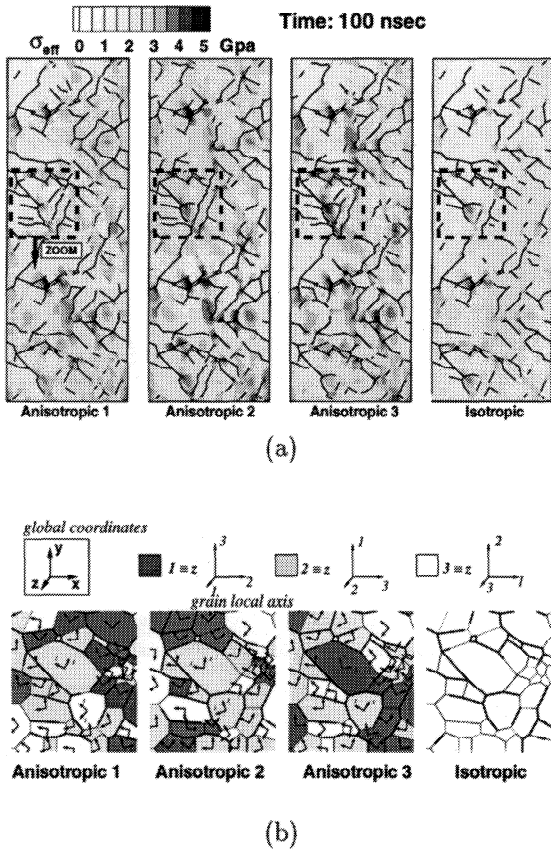


FIGURE 6: Effect of grain anisotropy: (a) Crack pattern showing the distribution of the effective Cauchy stress σ_{eff} for the three cases with grain elastic anisotropy and the case with elastic isotropy. (b) Zoom showing crack pattern and grain orientations.

and vice versa.

For instance the Weibull distribution for T_{max} is: $f(T_{max}) = \frac{m(T_{max}^0)^{m-1}}{T_{max}^0} \exp \left[- \left(\frac{T_{max}}{T_{max}^0} \right)^m \right]$. Where K_{IC}^0 and T_{max}^0 are material constants and m is the Weibull modulus which is a measure of the variability of the strength of the interface. Generally, $m = 5$ to 10 for the case of brittle ceramic samples.

The distribution will be such that a grain facet will have same interface element parameters, in this way there will be only N_f different interface elements ($N_f =$ number of facets in the microstructure). For the case where we

vary K_{IC} , the Weibull parameters are $K_{IC}^0 = 4MPa \cdot m^{1/2}$ and $T_{max} = 1GPa$. And two values of m are taken as $m = 3.6$ (where the Weibull distribution approximates the normal distribution) and $m = 10$. For the other case, $K_{IC} = 4MPa \cdot m^{1/2}$ and $T_{max}^0 = 1GPa$.

Since the interface parameters are randomly assigned, two simulations with different seeds were carried out for each one of these four distributions. This makes a total of 8 simulations. All the simulations are done with the same microstructure having the same principal material direction distribution.

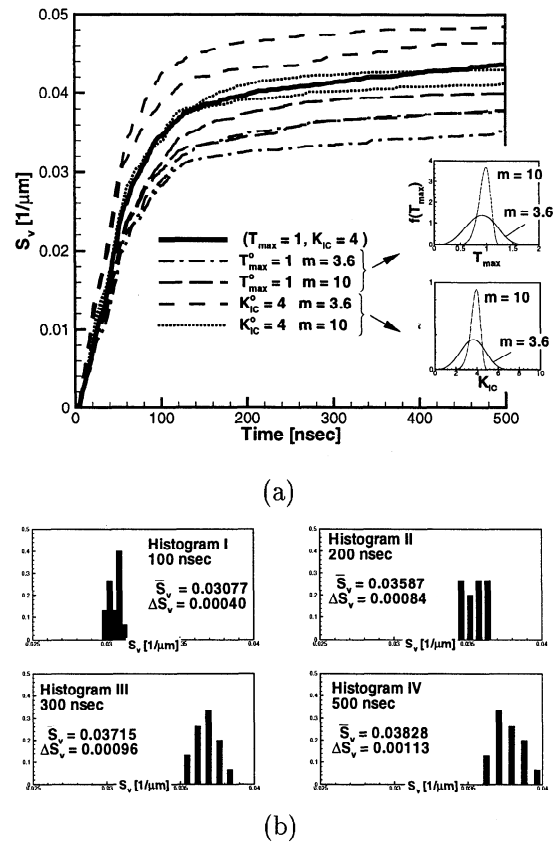


FIGURE 7: (a) Crack length per unit area for each distribution. (b) Effect of interface properties stochastic distribution for 15 runs with $T_{max}^0 = 1GPa$ and $m = 10$.

Figure 7(a) shows the crack length per unit

area, S_v , for each pair of the four different distributions. In order to compare, in the same curve the evolution of S_v for the case with interface with constant K_{IC} and T_{max} is shown. The overall response for the cases with the distribution $f(K_{IC})$ seems to be weaker than the cases with distribution $f(T_{max})$. The weakest case presents a 12% increment in the crack density with respect to the case without interface parameter variation, while the strongest case presents a 20% decrement. A statistical analysis has been done for one of the previous cases. The distribution $f(T_{max})$ with $K_{IC} = 4MPa \cdot m^{1/2}$, $T_{max}^0 = 1GPa$ and $m = 10$ was utilized in order to carry out fifteen simulations with different seeds. Figure 7(b) shows the histograms of $S_v(t)$ for different times. The mean value $\overline{S_v(t)} = (\sum_n S_v^i)/n$ and the standard deviation $\Delta S_v(t) = \sqrt{(\sum_n (S_v^i - \overline{S_v})^2)/n}$ are also shown in the figure.

Effect of grain morphology

It is well established that the grain structure in polycrystalline solid can be simulated by a Voronoi tessellation. In order to study the effect of grain morphology, Voronoi tessellation is utilized to generate different randomly shaped microstructures. Then, they are subjected to the same loading conditions. Figure 8 shows one of the ten microstructures generated using Voronoi tessellations. The same Figure also shows the crack length per unit area compared with the original case, i.e., digitized microstructure. A histogram of S_v at 500 nanoseconds is shown in the same figure. The mean $\overline{S_v}$ and the standard deviation ΔS_v are $0.0426/\mu m$ and $0.0061/\mu m$, respectively. The effect of the grain shape on the crack density is significant, not only for the final crack density, but also for its growth rate.

CONCLUDING REMARKS

The calculations presented in this article present assumptions that limit the degree of achievable accuracy. For instance, the calculations are 2-D instead of 3-D. As a result, a true random orientation of grains cannot be achieved

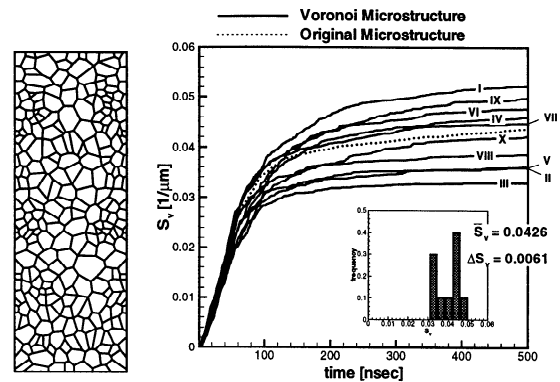


FIGURE 8: Voronoi microstructure and crack length per unit area compared with the original case with the digitized microstructure.

in the representative volume element. In the present analyses, the main damage and failure mode investigated was microcracking. However, in cases of stronger waves, visco-plasticity and twinning can be expected to become significant. Future modeling work will attempt to include these features. The goal is still the development of models capable of predicting inelasticity in ceramic materials on a variety of quasi-static and dynamic applications.

ACKNOWLEDGMENTS

This research was supported by the National Science Foundation through Career Award Nos. CMS 9523113, CMS-9624364, the Office of Naval Research YIP through Award No. N00014-97-1-0550, the Army Research Office through ARO-MURI Award No. DAAH04-96-1-0331 and the Air Force Office of Scientific Research through Award No. F49620-98-1-0039.

REFERENCES

1. Espinosa, H.D., Zavattieri, P.D., and Dwivedi, S., *J. Mech. Phys. Solids*, **46**, 10, pp. 1909-1942, 1998.
2. Zavattieri P.D., Raghuram, P., and Espinosa, H.D., submitted to *J. Mech. Phys. Solids*, 1999.
3. Espinosa H., Patanella A., Xu Y., submitted to *Experimental Mechanics*, 1999.